INTERFACE SCIENCE 6, 155–164 (1998)
© 1998 Kluwer Academic Publishers. Manufactured in The Netherlands.

Dynamics of Martensitic Interfaces

M. GRUJICIC
Department of Mechanical Engineering, Clemson University, Clemson, SC 29634-0921, U.S.A.
mica@ces.clemson.edu

G.B. OLSON
Department of Materials Science and Engineering, Northwestern University, Evanston, IL 60208-3108, U.S.A.

Abstract. The basic dynamic behavior of martensitic interfaces has been analyzed within the framework of lattice dislocation dynamics. Two limiting cases of the martensitic interface structure have been considered: (a) the case when the interface can be appropriately described in terms of an array of non-interacting (well-spaced) interfacial dislocations and; (b) the case when the interfacial dislocations are so closely spaced that the interface can be approximated by a continuous distribution of dislocations. In the first case, it was demonstrated that, after the inclusion of a "chemical" driving force in the equation of motion, the dynamics of lattice dislocations can be directly applied to analyze the interfacial dynamics. In the second case, on the other hand, while the lattice dislocation dynamics is still quite relevant, several parameters in the equation of motion have to be redefined to reflect the fact that the interface now acts as a planar defect. For both of the cases of interfacial dislocation structure, we have analyzed the two basic modes of interfacial motion: (a) the continuous mode in which the motion is controlled by various energy-dissipative processes (e.g., phonon and electron drag) and; (b) the discontinuous or jerky mode in which the motion is controlled by the thermal activation of the interface/obstacle interactions.

Keywords: martensitic interface, dynamics, thermal activation, phonon drag

1. Introduction

It is well-established that the analysis of martensite growth must include a consideration of the following two fundamental phenomena: (a) dynamics of interfacial motion and: (b) accommodation of transformation strain under consideration of variant selection. The structural changes occurring during the transformation require special interfaces between the parent phase and martensite, whose dynamics holds the key to many kinetic aspects of transformation. On the other hand, accommodation of the transformation strain may control morphological development of a martensite plate. While in the case of non-thermoelastic martensite, there is a dynamic interaction between the interfacial dynamics and plastic accommodation of the transformation strain which may govern the path of martensite growth, in the present paper only the interfacial dynamics will be discussed.

2. Interfacial Dynamics

2.1. Driving Forces due to Transformation Acting on an Interface

The proposed dislocation models for martensitic interfacial structure suggest that the dynamics of interfacial motion can be analyzed using the formalisms developed to describe dislocation dynamics. A general dislocation description of the martensitic interface has been developed by Olson and Cohen [1, 2] and Olson [3] who introduced two types of interfacial dislocations: (a) the "coherency dislocations" which, as they move with the interface, accomplish the lattice deformation while maintaining the continuity of crystal planes and directions across the interface and; (b) the "anticoherency dislocations" which, being true lattice discontinuities, disrupt the lattice continuity and, as they move, produce the lattice invariant deformation in

martensite. A simultaneous operation of the two deformation modes, the lattice deformation and the lattice invariant deformation, leave the interface plane macroscopically invariant, i.e., undistorted and unrotated.

Before the basic dynamics of interfacial motion can be analyzed, the forces acting on the interface must be defined. If no external stress is applied, the "driving" force for transformation can be defined as the volume Gibbs free energy difference between the martensite and parent phase, Δg_{ch}. Since the martensitic transformation is accompanied by a "transformation" strain, ε_{ij}^T, if an external stress, σ_{ij}^T, is applied to the crystal during transformation and concomitant energy-dissipative processes neglected, a work of transformation per unit volume of martensite formed can be defined as $\sigma_{ij}\varepsilon_{ij}^T$. It is a common practice [1, 2] to treat this work as the mechanical equivalent of a Gibbs free energy change Δg_σ. The total free energy change associated with formation of a unit volume of martensite Δg can thus be defined as:

$$\Delta g = \Delta g_{\text{ch}} + \Delta g_\sigma \tag{1}$$

Δg given by Eq. (1) can next be used to define an effective force per unit interfacial area acting in the direction of the interface normal (taken as the x direction) as:

$$F_A = -\frac{1}{A}\frac{dV}{dx}\Delta g \tag{2}$$

where A is the interfacial area and V the transformed volume corresponding to the interface displacement, x. For the motion of a rigid interface or for a small segment of the curved interface, the $1/A\ dV/dx$ term is unity and hence, Δg can be used as the interfacial driving force. The effect of the interfacial driving force and other forces such as the curvature (line or surface tension) force, and phonon and electron drag forces on interfacial motion is discussed in the next section.

2.2. *Equation of Motion*

When a lattice dislocation moves in response to a force $F = \tau^A b$, (τ^A is the resolved shear stress on the slip plane in the direction of the Burgers vector b), the dependence of the crystal energy on the dislocation position gives rise to a friction force $\tau_f b$ which apposes the dislocation motion. The friction stress τ_f varies markedly with the dislocation position and its peak values define a mechanical threshold stress $\hat{\tau}_f$. The net driving force acting on the dislocation is then given as $F_1^{\text{net}} = (\tau^A - \tau_f)b$. For a curved dislocation, the net force has to be modified to include the effect of the curvature force. If the relativistic effects are neglected the motion of a dislocation can be described by the following Newton's equation of motion:

$$\begin{aligned} F_1^{\text{net}} &= \left(\tau^A - \tau_f\right)b + \varepsilon\frac{d^2x}{dy^2} \\ &= m_1\frac{d^2x}{dt^2} + B_1\frac{dx}{dt} + \frac{\alpha_1 C_0\, dx/dt}{1+\beta_1^2(dx/dt)^2} \end{aligned} \tag{3}$$

where ε is the line tension, d^2x/dy^2 the dislocation curvature, x the direction of motion, y the overall dislocation direction, m_1 the dislocation inertial mass, B_1 a temperature-dependent phonon drag coefficient, α_1 and β_1 the temperature-dependent solute drag coefficients, and C_0 the solute concentration [7, 8]. The last term in Eq. (3) correctly predicts that at high interfacial velocities the effect of solute drag becomes insignificant. The same equation of motion can be used to described the motion of an interface consisting of an array of well-spaced interfacial dislocations, provided a chemical driving force contribution, $-\Delta g_{\text{ch}} \cdot s$, is added to F_1, where s is the interfacial dislocation separation. It should be noted that in many cases the martensitic interface velocity can become comparable with the speed of sound. In such cases, the relativistic effect can become significant and they can be accounted for by replacing the dx/dt term in Eq. (3) with $(dx/dt)/\{1-[(dx/dt)/c]^2\}^{1/2}$ where c is the speed of sound.

For an interface whose structure can be better approximated by a continuous distribution of dislocations, Eq. (3) has to be modified to replace the line (dislocation) parameters with the corresponding parameters for the two-dimensional interface as:

$$\begin{aligned} F_A^{\text{net}} &= -(\Delta g - \Delta g_f) + \gamma K \\ &= m_a\frac{d^2x}{dt^2} + B_a\frac{dx}{dt} + \frac{\alpha_a C_0\, dx/dt}{1+\beta_1^2(dx/dt)^2} \end{aligned} \tag{4}$$

Here $-\Delta g_f$ represents a frictional force, γ the (isotropic) surface tension, K the mean principal curvature, m_a the interfacial inertial mass, and B_a, α_a and β_a the corresponding drag coefficients.

It is customary to distinguish between two basic modes of interfacial (dislocation) motion [4]: (a) a continuous motion and; (b) a discontinuous or jerky motion. When the net driving force defined by Eqs. (3)

and (4) is positive everywhere in the crystal, the interfacial motion is continuous and is dominated by various energy-dissipative drag mechanisms. Conversely, when the driving force does not exceed the mechanical threshold, the interface reaches a state of static equilibrium when the local net driving force falls to zero. For the interface to continue to move, the interfacial atoms must acquire enough kinetic energy to overcome the local interfacial friction barrier. Once the interface has overcome the barrier, the interfacial driving force becomes positive and the interface begins to accelerate, until another barrier is encountered where the interfaces comes to rest again. The interfacial motion is thus microscopically discontinuous or jerky. Except at the stress level very close to the mechanical threshold, the overall rate of discontinuous interfacial motion is governed by the time it takes the interface to overcome the barrier by the assistance of thermal activation.

2.3. *Continuous Motion*

As stated earlier, the dynamics of continuous interfacial motion is governed by energy-dissipative processes, the main two being phonon drag and solute drag. In the following we give a brief overview of the phonon and solute drag controlled interfacial dynamics. According to Kocks et al. [4], various proposed phonon drag mechanisms all lead to the following general expression for the dislocation drag coefficient:

$$B_1 = \alpha\delta\frac{kT}{\Omega c} \tag{5}$$

where α is a geometrical factor obtained by integrating over the angular distribution of incident phonons around the dislocation, δ the scattering cross section per unit length, k the Boltzmann's constant, T the absolute temperature, Ω the atomic volume, and c the shear wave velocity. The magnitude of α is affected by the longitudinal to shear wave velocity ratio, and for metals it is usually assumed to be around 0.1. The magnitude of the scattering cross section δ and its dependence on frequency and temperature is affected by the type of phonon drag mechanism. The interfacial phonon drag coefficient B_a can be defined by a relation similar to Eq. (5), and using $\delta = 1$. As far as α parameter for an interface is concerned, its purely geometrical part is expected to be the same as that for a line dislocation. However, differences in the phonon modes in the two phases separated by the interface will, in general, affect the value of α. As an order-of-magnitude estimate one usually uses $B_a \approx B_1/d$, where d is the slip plane interplanar spacing of the interfacial dislocation.

Solutions of Eqs. (3) and (4) predict a steady-state phonon-drag controlled interfacial velocity which is a of the order of 50–60% of the shear wave velocity [5]. However, Yu and Clapp [6] demonstrated by carrying out magnetic and acoustic emission measurements that the interfacial velocities in Fe-30Ni are smaller by a factor of 2–3 than the predicted ones. This discrepancy was rationalized by taking into account the effect of the latent heat of transformation which raises the temperature in the region adjacent to the interface, and hence lowers the effective driving force. The temperature rise was shown to be as high as 92°C.

The effect of the solute drag on the interfacial dynamics has been analyzed by Owen et al. [7, 8]. The solute drag is the result of the elastic interaction between asymmetric strain centers associated with the interstitial solute atoms with the stress field of the moving interface. As a result of this interaction, the energy of the crystal is reduced by one of the following two processes: (a) rearrangement of the solute atoms by single jumps into the energetically most favorable, crystallographically equivalent neighboring sites, "The Snoek Interaction" [13, 14], or; (b) the solute diffusion over many atomic distances with the most favorable site being chosen at any distance from the interface, "The Cottrell Interaction" [11, 12]. During the time required for the solute atoms to redistribute by either of the two processes, the interface moves a short distance so that the solute atoms do not longer reside in the most favorable sites relative to the new position of the interface. As a result, the solute redistribution is out of phase with the instantaneous low-energy configuration of the system and an energy dissipation occurs, giving rise to an interfacial force.

Owen et al. [7, 8] adopted the solute drag model discussed above to rationalize the slow isothermal growth of martensite in Fe-10Ni-C alloys. The elastic interaction of the strain fields of dissolved carbon atoms in the martensite lattice with the stress field of the moving martensitic interface was determined for a specific dislocation model of the interface, which is consistent with the transformation crystallography. The analysis of the Snoek interaction showed that the resulting drag force is quite insignificant relative to that produced by the Cottrell interaction. To qualify the drag force arising from the Cottrell interactions, Owen et al. [7, 8] analyzed the long-range diffusion of solute atoms

to a moving interface which results in a steady-state solute concentration profile, known as the Cottrell atmosphere. This profile is obtained by solving the following differential equation:

$$v_R = -\frac{D}{kT}\frac{\partial w}{\partial x} - \frac{D}{C_0}\frac{\partial C_0}{\partial x} - v \qquad (6)$$

where v_R is the interface velocity relative to the solute atoms in the atmosphere, D the diffusion coefficient, w the solute/interface elastic interaction energy, v the interface velocity, and the appropriate boundary and continuity conditions are applied to Eq. (6). The total solute drag force is then obtained by integrating the solute/interface interaction forces over the volume of the Cottrell atmosphere. While a closed-form solution for the drag force is obtainable only in the limits of low and high interfacial velocities, Owen et al. [7, 8] used the approximate solution of Cahn [13] which is applicable in the entire interfacial velocity range. This solution, conveniently normalized to the unit dislocation length or unit interfacial area, is given respectively by the last terms in Eqs. (3) and (4).

Results obtained by Owen et al. [7, 8] for the drag force/velocity curves at 723 K for the Cottrell interaction of carbon atoms with the martensite interface in Fe-10Ni-C alloys with various carbon levels are shown in Fig. 1. It should be noted that for a typical driving force level of, 1090 J/mol (260 cal/mol), at the martensite start temperature M_s, none of the alloys experiences an instability in the interfacial motion. In other words, a stable equilibrium exits between the driving

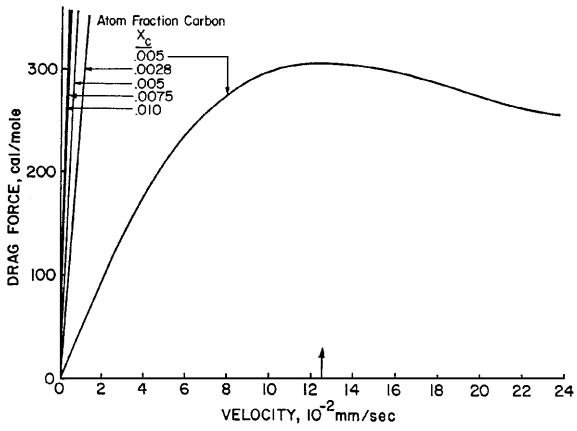

Figure 1. Calculated force-velocity curves for the Cottrell interaction of carbon atoms with the massive martensite boundary at 723 K for various carbon levels in Fe-10Ni-C [8].

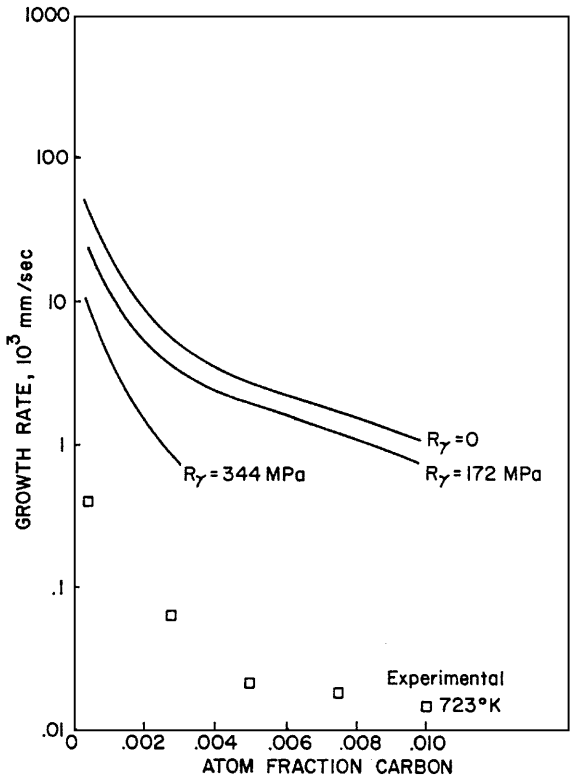

Figure 2. Comparison of the experimental and theoretically calculated width growth rates for Fe-10Ni-C alloys at 723 K [8].

and the drag forces giving rise to lower growth rates, the behavior which was confirmed experimentally. The results shown in Fig. 1 further suggest that, except for the alloys with the lowest carbon level, the drag force is, to a good approximation, a linear function of the interfacial velocity.

A comparison of the calculated and the measured interfacial velocities in Fe-10Ni-C alloys at 723 K is given in Fig. 2. The three calculated curves correspond to three different levels of an additional friction stress, R_γ. The magnitude of the friction stress is assumed to be independent of the velocity of the interface and, hence, it simply lowers the net interfacial driving force. The model predicts a steep drop in growth rate with the initial small addition of carbon, in excellent agreement with the experimental observations. However, the predicted interfacial velocity are one to two orders of magnitude higher than the measured ones with the extent of discrepancy depending on the magnitude of the additional frictional force assumed. While the improvements in the agreement between the predicted and measured velocities can be significantly improved

by adjusting the core cut-off radius and the diffusion coefficient, the use of linear elasticity to analyze the solute/interface interactions appears to be the main cause of the observed discrepancy. Namely, when the non-linear elasticity effects are taken into account, a significantly different Cottrell diffusion profile is obtained which increases the interfacial drag force and, in turn decreases the interfacial velocity.

2.4. *Thermally Activated Motion*

The basic concept of thermally activated dislocation motion can be understood by analyzing the schematic dislocation/obstacle interaction force-distance profile depicted in Fig. 3. Representing the position of a dislocation segment by the area swept during its motion, a, the variation of the internal friction stress with the position defines a τ vs. a profile of the form given in Fig. 3(a). For an applied stress τ^A, the dislocation is in stable equilibrium at point a_1. To reach the point a_2 of unstable equilibrium, the dislocation must overcome its activation energy Q_1 defined by the shaded area under the curve in Fig. 3(a). During such a thermally activated event, the dislocation line sweeps an "activation area" a^*, whose magnitude is a function of τ^A, as shown in Fig. 3(b). The activation energy can be obtained by the following integration:

$$Q(\tau^A) = b \int_{a_1}^{a_2} (\tau - \tau^A)\, da = \int_{\tau^A}^{\hat{\tau}} a^*\, d\tau \qquad (7)$$

The overall velocity of the dislocation in the thermally-activated region, v, is governed by the rate at which the dislocation overcomes the barrier and is defined as:

$$v = v_0 \exp\left(-\frac{Q}{kT}\right) \qquad (8)$$

where the pre-exponential factor v_0 is proportional to the corresponding attempt frequency. The two activation parameters, the activation area and the activation energy and their dependence on the applied stress can be determined from experimental dislocation mobility data using the relations:

$$Q = \left.\frac{\partial \ln v}{\partial(-1/kT)}\right|_{\tau^A} \qquad (9)$$

$$a^* = \frac{kT}{b}\left.\frac{\partial \ln v}{\partial \tau^A}\right|_T = -\frac{1}{b}\left.\frac{\partial Q}{\partial \tau^A}\right|_T \qquad (10)$$

When an interface consists of an array of well-spaced dislocations, the τ vs. a^* profile for the interfacial dislocations can be used to describe the interface/obstacle interaction. Conversely, when the interface is more appropriately described in terms of a continuous distribution of dislocations, the thermally activated event is three-dimensional in nature. For this case Grujicic et al. [14, 15] introduced an "activation volume" V^* as:

$$V^* = \left.\frac{\partial Q}{\partial \Delta g}\right|_T \qquad (11)$$

and demonstrated that the thermal activation analysis of the interfacial motion can be formulated in terms of the corresponding Δg vs. V^* profile. For an interface consisting of well separated dislocations, V^* can be defined in terms of a^* through the relation:

$$V^* = da^* \qquad (12)$$

When an obstacle profile such as the one shown in of Fig. 3 pertains to long-range interface/obstacle

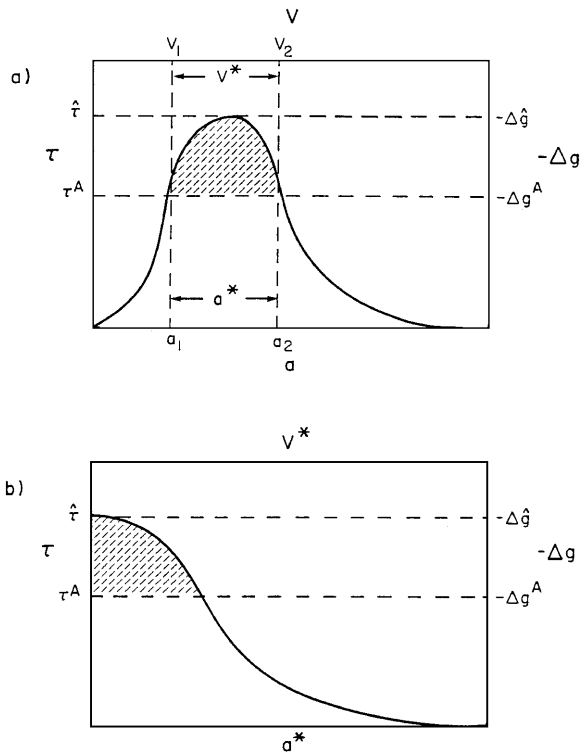

Figure 3. Schematic dislocation/obstacle interaction profiles. (a) Force-distance profile. (b) "Sheared profile" representing stress vs. activation area or driving force vs. activation-volume relation [15].

interactions, V^* becomes very large and consequently, the role of thermal activation becomes less important. If the interface can be described in terms of an array of well-spaced dislocations, the interface/obstacle interactions result in a velocity-invariant friction stress τ_μ which oppose the interface motion by lowering the net applied stress. In other words, the "thermal" component of τ^A that can assist thermal activation of the dislocation over short-range obstacles now becomes $\tau^A - \tau_\mu$. When several short-range obstacles simultaneously interact with an interface, the overall obstacle profile can be defined by the root sum of the squares of the individual profiles. Again, when the interface is more appropriated represented by a continuous distribution of dislocations, the athermal and the thermal components of the interfacial force should be defined in terms of Δg rather than τ.

Interfacial Motion Through a Perfect Crystal. As a dislocation moves through a perfect crystal, its core energy varies in a periodic manner due to the translational symmetry of the lattice. The resulting periodic lattice friction force, the Peierls barrier, can become the rate-controlling mechanism of dislocation motion at lower temperatures. When an interface can be described in terms of well separated dislocations, the interfacial dislocations may be considered to interact individually with the periodic lattice potential in much the same manner as the lattice dislocations. The energy of an edge dislocation as a function of position x can then be defined as:

$$E(x) = \frac{\mu b^2}{2\pi(1-\upsilon)}[1 - \alpha_p \cos(2\pi x/\lambda_0)] \quad (13a)$$

$$\alpha_p = \frac{\exp(-4\pi\delta_c/\lambda_0)}{\ln(R/\delta_c)} \quad (13b)$$

where δ_c is the effective dislocation core width and R the range of the dislocation stress field, usually taken as the average dislocation spacing in the crystal, and λ_0 the lattice periodicity. The energy $E(x)$ of a screw dislocation is obtained by omitting factor $(1-\upsilon)$ in Eq. (13a). The parameter α_p, which determines the amplitude of the energy variation, is affected by the choice of δ_c. The interaction of an isolated lattice dislocation with the periodic potential defined by Eq. (13) gives an activation energy, Q, proportional to b^2 and an activation volume, V^*, proportional to $\alpha_p^{-1/2}$. Therefore for comparable δ_c, the motion of interfacial coherency dislocation whose Burgers vector is only a small fraction of the lattice parameter involves comparable activation volumes but a significantly smaller Peierls barrier relative to that for lattice dislocations.

For the case of an interface which can be more appropriately defined in terms of a continuous distribution of dislocations, formation of a three-dimensional bulge over the Peierls barrier has been analyzed by Grujicic et al. [15, 16]. Under the assumptions of an isotropic interfacial tension γ_0 and a quasi-parabolic periodic variation of the interfacial energy γ with the interface position x/γ:

$$\gamma = \gamma_0 = 4\Delta\gamma\left(\frac{x}{\lambda_0}\right)\left(1 - \frac{x}{\lambda_0}\right) \quad (14)$$

where $\Delta\gamma/\gamma_0$ represents the amplitude of the interfacial energy variation (analogous to α_p in Eq. (13)), the following expressions were obtained:

$$Q = \frac{\pi^3}{4}\gamma_0\lambda_0^2(1 - \Delta g/\Delta\hat{g})^2 \quad (15)$$

$$V^* = \frac{\pi^3}{16}\frac{\lambda_0^3}{(\Delta\gamma/\gamma_0)}(1 - \Delta g/\Delta\hat{g}) \quad (16)$$

As in the case of isolated interfacial dislocations, the amplitude $\Delta\gamma/\gamma_0$ is sensitive to the choice of the interfacial core width δ_c. According to the nonlinear elastic strain-gradient energy model developed by Olson and Cohen [2], δ_c can be defined as:

$$\delta_c = (\chi/\Phi_0)^{1/2} \quad (17)$$

where χ is a gradient energy coefficient and Φ_0 is the threshold in strain-energy density associated with the homogeneous lattice deformation resulting from the motion of coherency dislocations. When a lattice is on the verge of mechanical instability, the effective Φ_0 could be quite low, giving rise to a high value of δ_c and the interface becomes diffuse. This, in turn, greatly reduces the height of the Peierls barrier. However, TEM observations of the martensitic interface core in metallic systems made by Chen and Olson [18], suggest, that δ_c is comparable to that of the lattice dislocations. Consequently, if a $\Delta\gamma/\gamma_0$ is taken to have a similar value as α_p for lattice dislocations (10^{-4} to 10^{-3}), Eq. (16) predicts relatively large values of the activation volume of $\sim 10^4$ Ω. Furthermore, if γ_0 is assigned a value between 10 and 50 mJ/m^2 which is a typical range for the martensitic interfaces in metallic systems, Eq. (15) predicts a maximum value of the activation energy of only $\sim 10^{-5}$ eV. This suggests that

the Peierls barrier does not have a major effect on controlling the motion of a martensitic interface. Nevertheless, one may expect that at the nucleation stage and under weak driving forces the role of the Peierls barrier may become more important.

Martensitic Interface Dynamics Controlled Interaction with Crystal Defects. While the effect of the Peierls barrier may be important in the growth of microscopic martensite particles under weak driving forces as suggested above, the motion of an interface of macroscopic dimensions, just like the motion of lattice dislocations, is more likely controlled by its interaction with crystal defects. For example, it is well established that cutting of repulsive forest dislocations by other dislocations, which involves generation of elementary jogs, gives rise to a significant strain hardening of metals at moderate temperatures. Likewise, the interaction of dislocations with attractive forest dislocations gives rise to long-range athermal friction stresses which oppose dislocation motion. Similar line-line interactions are expected to control the interfacial dynamics when the interface structure is dominated by well-spaced anticoherency dislocations. The interactions of closely spaced coherency dislocations with forest dislocations, can also be important but this interaction, should be treated as a line-surface problem.

Since the interface can interact with remote forest dislocation, the resulting interfacial friction stress is predominantly of the long range character and, thus, athermal. Similar conclusions can be drawn for surface-surface interactions involving the martensitic interface and other surface defects, such as antiphase boundaries. It should be noted that besides giving rise to additional (athermal) friction stresses, the line-surface and surface-surface interactions may be of a potential importance in assisting the generation of coherency dislocations by a pole mechanism during thickening of small martensitic particles.

The defects that most likely control thermally activated interfacial motion are discrete defects which take part in point-surface interactions. These interactions can be both a long-range (athermal) character as well as of the short-range (thermal) character. The interaction of an interface with regularly distributed. localized discrete particles, with average planar spacing λ (Fig. 4), has been analyzed by Grujicic et al. [15]. For a simplified dislocation model of interfacial structure, and using the analytical expressions for the corresponding interfacial stress field, Grujicic et al. [15] derived

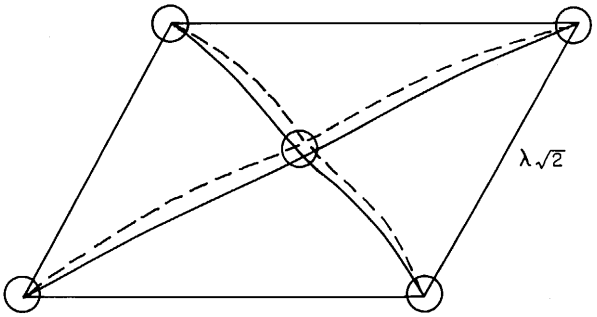

Figure 4. Schematic representation of the interaction between an interface and regularly distributed discrete particles with average planar spacing λ [15].

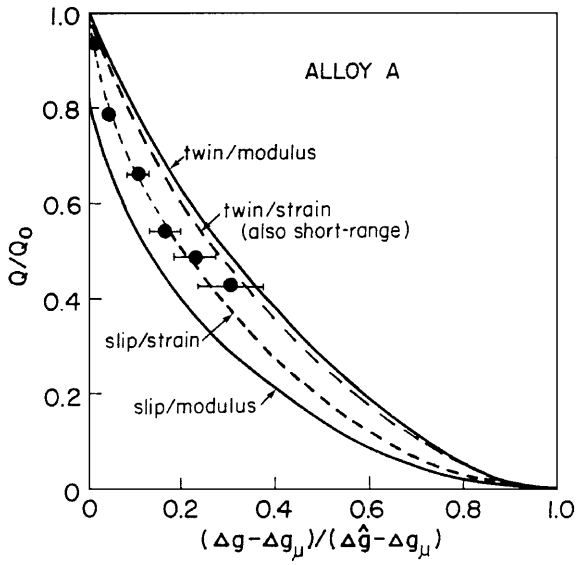

Figure 5. Normalized activation energy vs. driving force plot showing a comparison between different model predictions and the experimental mobility data in a Cu-14.3Al-4.0Ni single crystal [16].

the driving force vs. activation volume obstacle profiles for long- and short-range strain and modulus interface/obstacle interactions. Furthermore by applying an integration procedure analogous to the one indicated by Eq. (7), the corresponding Q vs. Δg relations were derived. The results of this procedure are shown in Fig. 5. Labels "slip" and "twin" were used in Fig. 5 to indicate the nature of the lattice-invariant deformation. It is customary to represent the Q vs. Δg relations as the ones shown in Fig. 5, by the following expression:

$$Q = Q_0\left[1 - \left(\frac{\Delta g - \Delta g_\mu}{\Delta \hat{g} - \Delta g_\mu}\right)p\right]q \qquad (18)$$

Table 1. Values of p and q exponents in Eq. (8) for various type of interface/particle interactions.

Lattice invariant deformation	Obstacle	Interaction	p	q
		Strain	1	2
Twinning	Discrete particle	Modulus	1	9/5
		Short range	1	2
	Peierls barrier	—	1	2
		Strain	1/2	3/2
Slip	Discrete particle	Modulus	4/5	2
		Short range	1	2
	Peierls barrier	—	1	2
Twinning	Experimental measurement of single interface mobility in Cu-14.3Al-4.0Ni [16, 17]		0.39	1.35

where Q_0 is the maximum activation energy, Δg_μ is the athermal part of Δg, and the exponents p and q describe, respectively, the long-range (small Δg) and the short-range (large Δg) interfacial/obstacle interaction behavior. The characteristic values of p and q for the various interface/particle interactions are summarized in Table 1.

The results shown in Fig. 5 and Table 1 suggest that the interaction of a "slip" interface with the same array of discrete obstacles, is significantly different than that of a "twin" interface.

Grujicic et al. [15] also found that the magnitudes of Q_0 and $\Delta\hat{g}$ are both substantially larger for a "slip" interface, than a "twin" interface. The last finding suggests that a "twin" interface is intrinsically more mobile than the "slip" interface.

Stress-assisted single-interface martensitic transformation in single crystals of thermoelastic alloys allows direct measurement of the interfacial dynamics. Such measurements have been carried out by Grujicic et al. [14, 15] using Cu-Al-Ni single crystals. Figure 6 shows the measured temperature dependence of the interfacial friction stress and the corresponding driving force for the interfacial velocities in the range between 10^{-6} and 10^{-3} m/s in a Cu-14.3Al-4.0Ni single crystal. Due to the experimental limitation, higher interfacial velocities could not be achieved and, hence, only the thermally activated regime of interaction motion was characterized. As indicated by the dashed line in Fig. 6, there is a well-defined athermal interfacial friction stress, τ_μ. The Δg vs. V^* and Q vs. Δg obstacle profile associated with the thermal part of the applied stress are shown in Figs. 7 and 8, respectively. The Q vs. Δg relation was found to be consistent with Eq. (18) with $Q_0 = 0.305$ eV, $-\Delta\hat{g} = 0.9$ MJ/m^3, $-\Delta g_\mu = 2.21$ MJ/m^3, $p = 0.39$, and $q = 1.35$. It should be noted that the observed values of p and q are in quite poor agreement with their model counterparts for the strain and modulus interactions of an internally twinned interface Table 1. The discrepancy was subsequently resolved

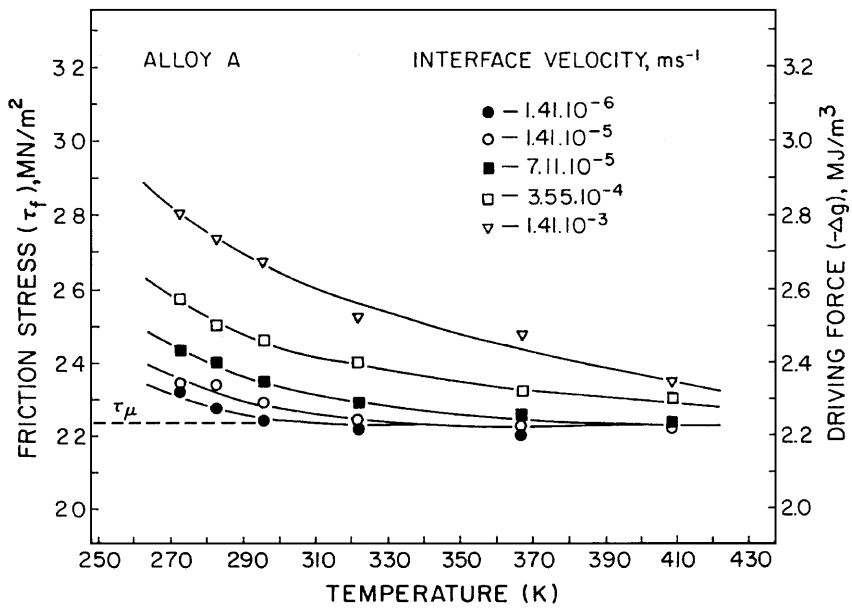

Figure 6. Temperature and velocity dependence of the friction stress (driving force) in a Cu-14.3Al-4.0Ni single crystal [16].

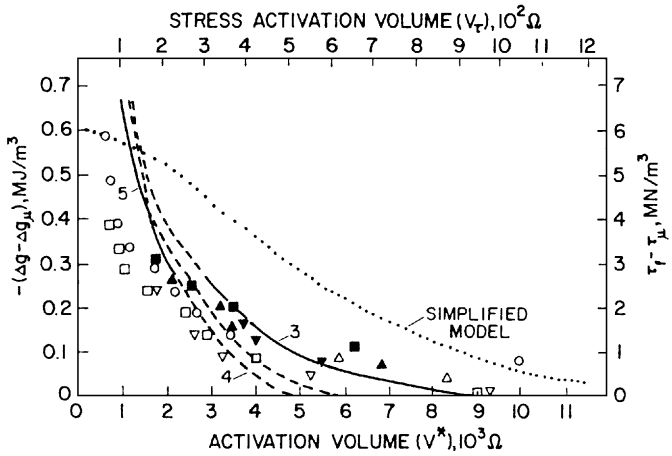

Figure 7. Comparison of the model predictions for the strain-interaction obstacle profile (solid lines) and the experimentally measured obstacle profile in a Cu-14.3Al-4.0Ni single crystal [17].

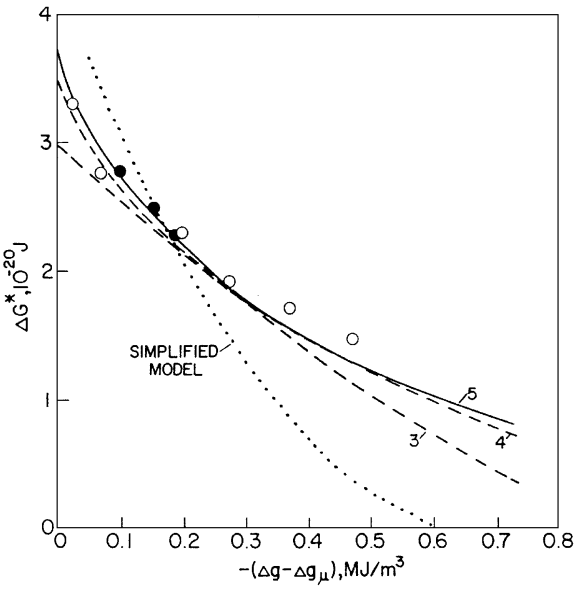

Figure 8. Comparison of the model prediction (solid curves) for the strain-interaction activation energy vs. driving force relation and the experimentally measured relations between activation energy and driving force in a Cu-14.3Al-4.0Ni single crystal [17].

by Grujicic et al. [17] who employed a interfacial dislocation model specific to the twinned $\beta_1 - \gamma_1'$ martensitic interface, instead of the simple general interface model previously used. By analyzing both the interfacial mobility data and the transmission electron microscopic results of the parent β_1-phase, Grujicic et al. [16] determined that the thermal-activated motion of the $\beta_1 - \gamma_1'$ interface is controlled by the "tweed" structure, consisting of high-modulation displacement fields. The athermal frictional stress, on the other hand, was attributed to be a long-range modulus interaction of the interface with discrete 2H precipitated in the β_1-phase.

In conclusion, while throughout this paper we used the dislocation dynamics framework to analyze the dynamics of martensitic interface, a word of caution is in order. In contrast to the motion of line dislocations, the motion of an interface, as in the case of growth of an enclosed martensitic particle, requires not only the motion of interfacial dislocations but also the regular generation of discrete dislocation loops. As discussed by Olson and Cohen [19], the activation energy for nucleation of discrete dislocation loops can be higher than that for the motion of the existing dislocation, and, thus, the rate of formation of dislocation loops becomes a potentially rate-controlling mechanism of particle growth.

Acknowledgment

The work has been supported by the National Science Foundation under Grants DMR-9317804 and CMS-9531930 at Clemson University and DMR-9500122 at the Northwestern University.

References

1. G.B. Olson and M. Cohen, Acta Metall. **27**, 1907 (1979).
2. G.B. Olson and M. Cohen, in *Proc. Int. Conf. Solid-Solid Phase Transformations*, edited by H.I. Aaronson (TMS-AIME, 1982), p. 1209.

3. G.B. Olson, Acta Metall. **29**, 1475 (1981).
4. U.F. Kocks, A.S. Argon, and M.F. Ashby, Prog. Mat. Sci. **19**, 1 (1975).
5. M. Grujicic, J. Mater. Sci. **32**, 10 (1997).
6. Z.Z. Yu and P.C. Clapp, Metall. Trans. **20A**, 1601 (1989).
7. W.S. Owen, F.J. Schoen, and G.R. Scrinivasan, in *Phase Transformations* (American Society for Metals, 1970), p. 157.
8. F.J. Schoen and W.S. Owen, Metall. Trans. **2**, 2431 (1971).
9. J. Snoek, Physics, **8**, 711 (1941).
10. G. Schoeck and A. Seeger, Acta Metall. **7**, 469 (1959).
11. A.H. Cottrell and B.A. Bilby, in *Proc. Phys. Soc.* (1949), vol. 62, p. 49.
12. A.H. Cottrell and M.A. Jaswon, in *Proc. Roy. Soc. Lond.* (1949), vol. A199, p. 104.
13. J.W. Cahn, Acta Metall. **10**, 789 (1962).
14. M. Grujicic, G.B. Olson, and W.S. Owen, J. Phys. (Suppl. 12) **43**, C4-173 (1982).
15. M. Grujicic, G.B. Olson, and W.S. Owen, Metall. Trans. **16A**, 1713 (1985).
16. M. Grujicic, G.B. Olson, and W.S. Owen, Metall. Trans. **16A**, 1723 (1985).
17. M. Grujicic, G.B. Olson, and W.S. Owen, Metall. Trans. **16A**, 1735 (1985).
18. F.-R. Chen and G.B. Olson, in *Proc. XIIth Intl. Conf. Electron Microscopy* (1990), p. 111.
19. G.B. Olson and M. Cohen, Metall. Trans. **7A**, 1915 (1976).